0026-895X/06/6903-788–795$20.00
MOLECULAR PHARMACOLOGY
Copyright © 2006 The American Society for Pharmacology and Experimental Therapeutics
Mol Pharmacol 69:788–795, 2006

Vol. 69, No. 3
18200/3090139
Printed in U.S.A.

How Batrachotoxin Modifies the Sodium Channel Permeation Pathway: Computer Modeling and Site-Directed Mutagenesis

Sho-Ya Wang, Jane Mitchell, Denis B. Tikhonov, Boris S. Zhorov, and Ging Kuo Wang

Department of Biology, State University of New York at Albany, Albany, New York (S.Y.W.); Department of Biochemistry and Biomedical Sciences, McMaster University, Hamilton, Ontario, Canada (D.B.T., B.S.Z.); and Department of Anesthesia, Brigham and Women's Hospital and Harvard Medical School, Boston, Massachusetts (J.M., G.K.W.)

Received August 23, 2005; accepted December 13, 2005

ABSTRACT

A structural model of the rNav1.4 Na^+ channel with batrachotoxin (BTX) bound within the inner cavity suggested that the BTX pyrrole moiety is located between a lysine residue at the DEKA selectivity filter (Lys1237) and an adjacent phenylalanine residue (Phe1236). We tested this pyrrole-binding model by site-directed mutagenesis of Phe1236 at D3/P-loop with 11 amino acids. Mutants F1236D and F1236E expressed poorly, whereas nine other mutants either expressed robust Na^+ currents, like the wild-type (F1236Y/Q/K), or somewhat reduced current (F1236G/A/C/N/W/R). Gating properties were altered modestly in most mutant channels, with F1236G displaying the greatest shift in activation and steady-state fast inactivation (−10.1 and −7.5 mV, respectively). Mutants F1236K and F1236R were severely resistant to BTX after 1000 repetitive pulses (+50 mV/20 ms at 2 Hz), whereas seven other mutants were sensitive but with reduced magnitudes compared with the wild type. It is noteworthy that rNav1.4-F1236K mutant Na^+ channels remained highly sensitive to block by the local anesthetic bupivacaine, unlike several other BTX-resistant mutant channels. Our data thus support a model in which BTX, when bound within the inner cavity, interacts with the D3/P-loop directly. Such a direct interaction provides clues on how BTX alters the Na^+ channel selectivity and conductance.

Batrachotoxin (BTX), a potent neurotoxin found in the skin of various poisonous frogs (Tokuyama et al., 1968; Daly et al., 1980; for review, see Brown, 1988), is a steroidal alkaloid with a tertiary amine (batrachotoxinin A 20-[2,4-dimethyl-1*H*-pyrrole-3-carboxylate]) (Fig. 1A). BTX specifically targets voltage-gated Na^+ channels and, when bound, drastically alters Na^+ channel properties (Hille, 2001). First, BTX shifts the activation gating to the hyperpolarizing direction by 30 to 50 mV. As a result, voltage-gated Na^+ channels open readily even at resting membrane potentials. Second, BTX eliminates both fast and slow inactivation gating. Consequently, single BTX-modified Na^+ channels remain open for hours, as recorded in planar lipid bilayers (Krueger et al., 1983). Third, BTX reduces the single channel conductance by ~50% (Correa et al., 1991). Fourth, BTX alters the ion selectivity of Na^+ channels (Khodorov, 1978). How BTX elicits all these changes simultaneously is not well understood.

Mammalian voltage-gated Na^+ channels contain one large α-subunit and one or two small β-subunits (Catterall, 2000). Nine α- and four β-subunit isoforms have been identified in mammals so far. The large α-subunit protein consists of four repeated domains (D1–D4), each with six transmembrane segments (S1–S6; Fig. 1B). The receptor for BTX within the Na^+ channel α-subunit has been delineated by site-directed mutagenesis (e.g., Linford et al., 1998; Li et al., 2002). Accumulated evidence suggests that all four S6 segments from D1–D4 may jointly form the BTX receptor within the inner cavity (Fig. 1B, closed arrow) (for review, see Wang and Wang, 2003). In contradiction, the receptor for local anesthetics seems to overlap the BTX receptor at D1S6, D3S6, and D4S6 (Nau and Wang, 2004). Three of the BTX-binding residues (D2S6, D3S6, and D4S6) are adjacent to the putative gating hinge (Gly/Ser residue at the middle of S6s; Fig. 1C, boxed), which may govern the channel opening, as suggested by the open configuration of MthK channels (Jiang et al., 2002). In addition to S6s, several residues in P-loops located within the S5/S6 linkers could also face the inner cavity, as

This work was supported by National Institutes of Health grants GM48090 and HL66076 (to G.K. and S.-Y.W.) and from the Canadian Institutes of Health Research (CIHR) (to B.S.Z.). B.S.Z. is the recipient of a CIHR Senior Scientist award.

Article, publication date, and citation information can be found at http://molpharm.aspetjournals.org.

doi:10.1124/mol.105.018200.

ABBREVIATIONS: BTX, batrachotoxin; rNav1.4, the rat skeletal muscle isoform of the Na^+ channel; DEKA, the four residues forming the putative selectivity filter (Asp, Glu, Lys, Ala); KcsA, K^+ channel from *Streptomyces lividans*; MthK, Ca^{2+}-activated K^+ channel from *Methanobacterium thermoautotrophicum*; MTSEA, methanethiosulfonate ethylammonium.

implied by the X-ray structures of KcsA (Doyle et al., 1998) and MthK (Jiang et al., 2002). However, no experimental evidence of the direct interaction of BTX with P-loop residues is available.

Tikhonov and Zhorov (2005b) recently suggested that BTX alters the structure of the ion selectivity filter (i.e., the DEKA locus), possibly by wedging its pyrrole moiety between Phe1236 and Lys1237 residues at the D3/P-loop. This structural configuration is based on computer modeling of the Na^+ channel permeation pathway, with BTX bound within the inner cavity. This model provides a testable hypothesis that BTX directly interacts with residues at the D3/P-loop within the inner cavity and suggests that residue Phe1236 interacts with the pyrrole group of BTX via π-π stacking. The purpose of this study is to test the validity of such a structural model using site-directed mutagenesis of the Phe1236 residue at the D3/P-loop.

Materials and Methods

Site-Directed Mutagenesis. We used the QuikChange XL site-directed mutagenesis kit (Stratagene, La Jolla, CA) to create rNav1.4-Phe1236 mutants within the pcDNA1/Amp vector (Wang et al., 2003). DNA sequencing around the mutated region confirmed the mutations.

Transient Transfection. Human embryonic kidney (HEK) 293t cells were grown to ~50% confluence in Dulbecco's modified Eagle's medium (Life Technologies, Inc., Rockville, MD) containing 10% fetal bovine serum (HyClone, Logan, UT), 1% penicillin and streptomycin solution (Sigma, St. Louis, MO), 3 mM taurine, and 25 mM HEPES (Life Technologies, Inc.), and then transfected by calcium phosphate precipitation. Transfection of wild-type or rNav1.4-Phe1236 mutants (5–10 μg) along with rat β1-pcDNA1/Amp (10–20 μg) and reporter CD8-pih3m (1 μg) was adequate for current recording. Cells were replated 15 h after transfection in 35-mm dishes, maintained at 37°C in a 5% CO_2 incubator, and used after 1 to 4 days. Transfection-positive cells were identified with immunobeads (CD8-Dynabeads; Dynal Biotech, Lake Success, NY).

Whole-Cell Voltage Clamp. Whole-cell configuration was used to record Na^+ current (Hamill et al., 1981). Borosilicate micropipettes (Drummond Scientific, Broomall, PA) were pulled (P-87; Sutter Instrument Company, Novato, CA) and heat-polished. Pipette electrodes contained 100 mM NaF, 30 mM NaCl, 10 mM EGTA, and 10 mM HEPES adjusted to pH 7.2 with CsOH. The pipette electrodes had a tip resistance of 0.5 to 1.0 MΩ. Access resistance was generally 1 to 2 MΩ. We minimized the series resistance (>85%) and corrected the leak and capacitance using the Axopatch 200B device (Molecular Devices, Sunnyvale, CA). Holding potential was set at −140 mV. Further correction was achieved by the P/-4 protocol.

Experiments were performed at room temperature (22–24°C) under a Na^+-containing bath solution with 65 mM NaCl, 85 mM choline chloride, 2 mM $CaCl_2$, and 10 mM HEPES adjusted to pH 7.4 with tetramethylammonium hydroxide. An unpaired Student's t test was used to evaluate estimated parameters (mean ± S.E.M. or fitted value ± S.E. of the fit); P values of <0.05 were considered statistically significant.

Drug Solutions. BTX, a generous gift from Dr. John Daly (National Institutes of Health), was dissolved in dimethyl sulfoxide at 0.5 mM and stored at −20°C. The final concentration of BTX was 5 μM in the pipette solution. Bupivacaine was obtained from Sigma (St. Louis, MO), dissolved in dimethyl sulfoxide at 100 mM, and stored at −20°C. Serial dilutions of bupivacaine were made with the bath solution.

Molecular Modeling. Molecular modeling of BTX bound within the inner cavity of the wild-type rNav1.4 Na^+ channel was performed as described by Tikhonov and Zhorov (2005a,b). Energetically optimal complexes of Phe1236 mutants with BTX were obtained by Monte Carlo minimization.

Results

Expression and Gating Properties of Phe1236 Mutant Channels in HEK293t Cells. The model of Tikhonov and Zhorov (2005b) predicted Phe1236 at the D3/P-loop region as an important component of the BTX receptor. To test this prediction, we performed extensive site-directed mutagenesis of Phe1236. Mutant rNav1.4-Phe1236 Na^+ chan-

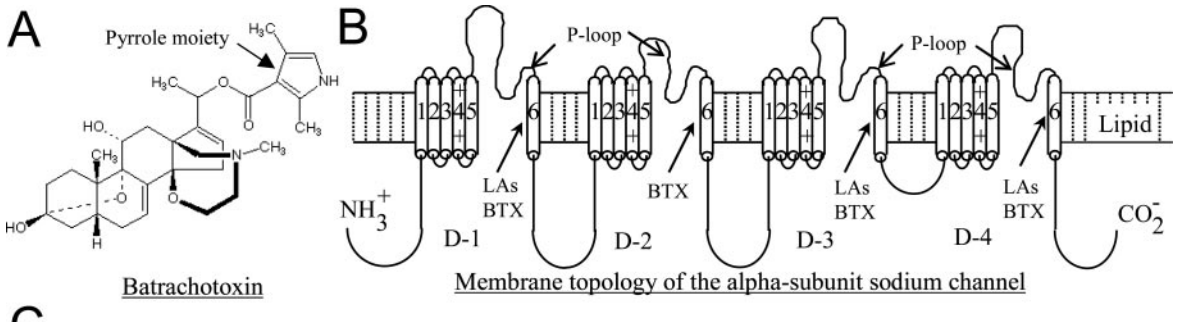

Fig. 1. A, the chemical structure of BTX. The pyrrole moiety is labeled (arrow). B, the membrane topology of the sodium channel α-subunit. Domains 1 through 4 each contain six transmembrane segments (S1–S6). Several S6 segments jointly form the receptors for BTX and LA within the inner cavity (closed arrows). The extracellular linker between S5 and S6 forms the P-loop (open arrows), which includes the selectivity filter. C, the amino acid sequences of P-loops and S6 segments are listed. The selectivity filter (i.e., DEKA locus) and residue Phe1236 at the D3-P loop are underlined and in bold. The position 12 (boxed) for the putative gating hinge is tentatively assigned, although no consensus on the S6 alignment has yet emerged. Residues Asn784 (D2S6) and Phe1579 (D4S6) are also in bold letters.

nels were expressed in HEK293t cells, and their gating properties were characterized under whole-cell, patch-clamp configuration. Families of Na^+ currents were recorded under various voltages (Fig. 2A). Peak currents were measured, converted to conductance, normalized, and plotted against voltage (Fig. 2B). The plots were fitted by Boltzmann equation, and the $E_{0.5}$ value and the slope factor (k) were determined. For rNav1.4-F1236K mutant channels, the shift in $E_{0.5}$ was minimal ($P < 0.05$). Other mutants were similarly characterized, and the shifts in activation were compared with the wild type as shown in Fig. 3A. Only F1236G mutation shifted the activation by approximately −10 mV, whereas the remaining mutations shifted ≤5 mV. Because F1236E and F1236D both expressed insufficient Na^+ currents (<50 pA/pF), these two mutants were not studied further. In contrast, all other mutant channels expressed ≥250 pA/pF (Fig. 3B) and were further characterized. Mutants F1236Y, F1236K, and F1236Q expressed robust Na^+ currents (~400 pA/pF) almost as large as those of the wild type.

Steady-state fast inactivation (h_∞) was determined by a conventional two-pulse protocol. Peak currents were measured, normalized with respect to the peak at −160 mV, and plotted against the conditioning voltage (Fig. 2C). The data were fitted by a Boltzmann equation to yield $h_{0.5}$ and the slope factor (k). No significant changes were found between wild-type and F1236K mutant Na^+ channels in h_∞ curves. Other mutants were similarly characterized and the shifts in $h_{0.5}$ values are listed in Fig. 3C.

Slow inactivation occurs considerably in muscle rNav1.4 Na^+ channels. To determine the magnitude of slow inactivation, we applied a 10-s conditioning pulse at various voltages. Approximately 45% of wild-type Na^+ channels were slow-inactivated at −40 to 0 mV (Fig. 2D, ■); these slow-inactivated channels were not recovered after a 100-ms interpulse at −140 mV. With this assay, we found that wild type, F1236K (Fig. 2D, □), and all other Phe1236 mutants remained susceptible to slow inactivation (Fig. 3D); several of them were even more susceptible than the wild-type channels.

Modifications of Mutant Na^+ Channels by BTX. We applied repetitive pulses to facilitate BTX binding because BTX can interact only with the open Na^+ channel. In the presence of 5 μM BTX within the pipette, wild-type rNav1.4 channels were modified by BTX during repetitive pulses. Figure 4A shows superimposed current traces recorded after 1, 100, 300, 600, and 1000 pulses in HEK293t cells expressing wild-type Na^+ channels. More than 75% of peak currents were modified by BTX and became noninactivating at the end of a 20-ms pulse.

In contrast, rNav1.4-F1236K mutant Na^+ currents seemed

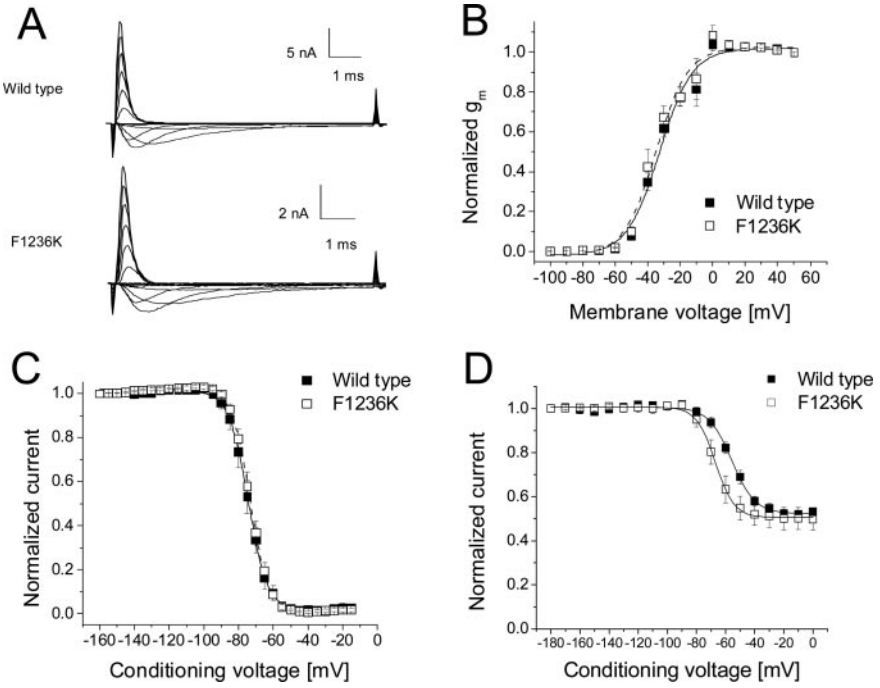

Fig. 2. Gating properties of wild-type and rNav1.4-F1236K mutant channels coexpressed with β1. A, families of superimposed Na^+ current traces at various voltages of wild-type (top) and rNav1.4-F1236K mutant (bottom) are shown. Peak Na^+ currents were measured, converted to conductance, normalized with respect to conductance at +50 mV, and plotted against voltage B. Conductance was determined by the equation $g_m = I_{Na}/(E_m - E_{Na})$, where I_{Na} is the peak current, E_m is the voltage applied, and E_{Na} is the estimated reversal potential. Plots were fitted with a Boltzmann function, which gave a midpoint voltage ($V_{0.5}$) and slope (k) for wild-type (■, $n = 5$) of −32.7 ± 1.4 and 10.0 ± 1.2 mV, respectively, and −34.9 ± 1.5 and 9.8 ± 1.3 mV for rNav1.4-F1236K (□, $n = 5$). Mutation of F1236K did not alter activation gating significantly. C, conventional steady-state inactivation (h_∞ curve) was measured by a two-pulse protocol. Currents were evoked by 5-ms test pulses to +30 mV after 100-ms conditioning pulses ranging from −160 to −15 mV in 5-mV increments. Peak currents at the test pulse were measured, normalized with respect to the peak current at the conditioning pulse at −160 mV, and plotted against conditioning voltages. The fitted midpoint ($h_{0.5}$) and slope factor (k) for the wild-type were −74.5 ± 0.5 mV and 5.5 ± 0.1 mV, respectively, and −73.3 ± 0.6 mV and 5.2 ± 0.1 mV, respectively, for rNav1.4-F1236K. Minimal changes were observed between wild-type (■, $n = 5$) and rNav1.4-F1236K mutant (□, $n = 5$). D, slow inactivation was measured by a 10-s conditioning pulse at voltages ranging from −180 to 0 mV. Currents were evoked by a 5-ms test pulse at +30 mV. Normalized currents were plotted against the conditioning voltage and fitted with a Boltzmann function. Slow inactivation in rNav1.4-F1236K mutant channels (□, $n = 5$) was enhanced and shifted to the hyperpolarizing direction compared with wild-type channels (■, $n = 5$). The fitted midpoint ($V_{0.5}$) and slope factor (k) were −55.7 ± 0.5 and 7.9 ± 0.5 mV, respectively, for the wild-type, and −67.1 ± 0.2 and 6.5 ± 0.3 mV, respectively, for rNav1.4-F1236K.

extremely resistant to BTX modification. Little or no maintained currents were recorded at the end of a 20-ms pulse (Fig. 4B). Another mutation with a positive charge, rNav1.4-F1236R, also showed a similar BTX-resistant phenotype (Fig. 5). All other mutant channels remained sensitive to BTX modification. F1236N and F1236C (Fig. 4C) mutant channels were modified by BTX nearly as effectively as the wild-type channels were, whereas F1236Q and F1236W were modified but with a significant reduced magnitude after 1000 pulses (Fig. 5; $P < 0.05$). The BTX sensitivity followed the order: Phe1236 > Asn ≈ Cys > Gly ≈ Ala > Tyr > Gln ≈ Trp > Arg ≈ Lys.

Block of BTX-Resistant F1236K Mutant Na^+ Channels by Bupivacaine. Previous studies showed that a number of BTX-resistant mutant Na^+ channels are also resistant to local anesthetic block in their inactivated state (Linford et al., 1998; Nau and Wang, 2004). It is noteworthy that Lys1237, the residue adjacent to the Phe1236 position mutated in the current study, strongly regulates the binding of local anesthetics (Sunami et al., 1997). We therefore assayed the sensitivity of the local anesthetic bupivacaine in F1236K mutant channels. Figure 6A shows that F1236K Na^+ currents were blocked by bupivacaine in a voltage-dependent manner. At −160 mV, most Na^+ channels were in their resting state and displayed weak block by bupivacaine at 100 μM (left). The resting block was further characterized at various bupivacaine concentrations, resulting in the dose-response curve shown in Fig. 6B. The IC_{50} value for the resting affinity of bupivacaine was estimated to be 162.3 ± 3.3 μM, with a Hill coefficient of 1.04 ± 0.06 ($n = 5$).

In contrast to the weak block by bupivacaine at −160 mV, the block was significantly stronger at −70 mV, where most Na^+ channels were in their inactivated state (Fig. 6A, right). The dose-response curve yielded an estimated IC_{50} value of 12.1 ± 0.9 μM with a Hill coefficient of 0.85 ± 0.05 ($n = 5$). However, both the IC_{50} values for the resting and for the inactivated states were indistinguishable from those measured in the wild-type channels (e.g., Nau et al., 1999). This result implies that, unlike BTX, bupivacaine does not interact with residue Phe1236 directly.

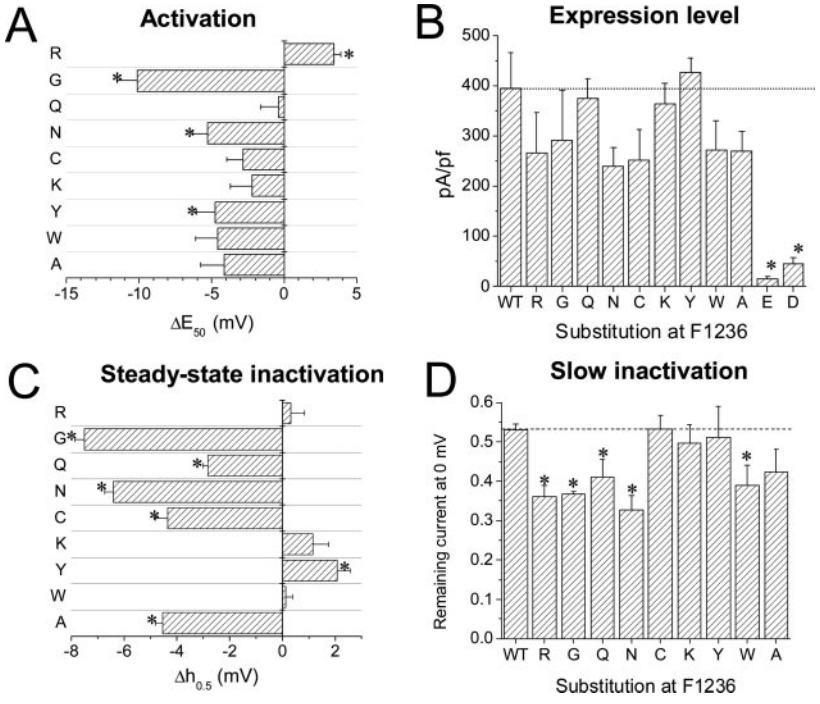

Fig. 3. Comparisons of gating properties in Phe1236 mutant channels. A, shifts in activation gating were measured as described in Fig. 2B. Differences in midpoint voltage ($E_{0.5}$) values obtained from Boltzmann fits ($n = 5$) were compared among wild-type and various Phe1236 mutants. B, the expression level of various Phe1236 mutant channels. Peak current amplitudes were measured at +50 mV and normalized with the membrane capacitance of individual cells. F1236E/D mutants expressed poorly. All values were derived from $n = 5$–6, except for the wild-type with $n = 7$, F1236K with $n = 12$, and F1236D with $n = 14$. C, shifts in steady-state inactivation were measured as described in Fig. 2C. All $\Delta h_{0.5}$ values were derived from $n = 5$–6. D, magnitudes of slow inactivation at 0 mV were measured as described in Fig. 2D. The dotted line indicates the wild-type value. All values were derived from $n = 5$. *, $P < 0.05$ compared with the value of the wild-type.

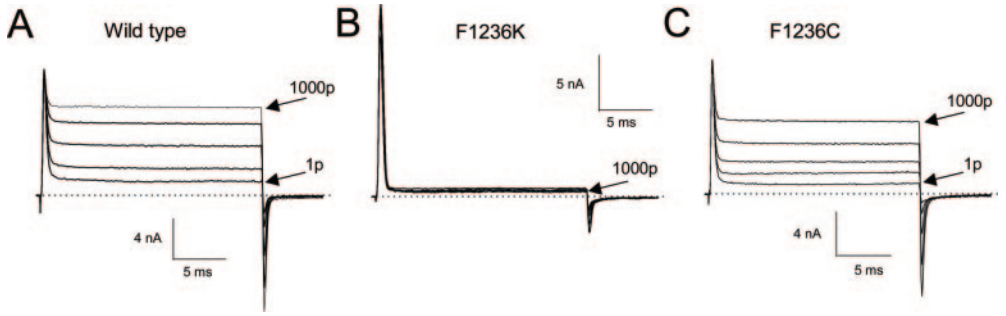

Fig. 4. Modification of Na^+ currents by BTX during repetitive pulses. Superimposed Na^+ current traces of wild-type (A), rNav1.4-F1236K (B), and rNav1.4-F1236C (C), mutant channels are shown after 1, 100, 300, 600, and 1000 depolarizing pulses at +50 mV for 20 ms. The amplitudes of maintained noninactivating Na^+ currents were progressively increased in wild-type and rNav1.4-F1236C Na^+ channels during repetitive pulses. In contrast, rNav1.4-F1236K channels were resistant to BTX modification; maintained noninactivating Na^+ currents were minimal after 1000 repetitive pulses. Peak currents of rNav1.4-F1236K were reduced during repetitive pulses, probably because of cumulative slow inactivation. Cells were dialyzed for ~15 min with infrequent test pulses before repetitive pulses.

Computer Modeling of the Na^+ Channel Permeation Pathway and BTX Bound Within the Inner Cavity. BTX-binding residues around the selectivity filter area have been implicated in the earlier structural model (Tikhonov and Zhorov, 2005b). This model is also consistent with results derived from site-directed mutagenesis of S6 residue (Wang and Wang, 2003). Figure 7A shows the pore helices and P-loop turns as green ribbons and rods, respectively. The ligand is shown as sticks. In this model, a phenylalanine residue (Phe1236; Fig. 7A, box) adjacent to lysine (Lys1237) at the D3/P-loop of the DEKA locus is situated near the pyrrole moiety of BTX. From a structural viewpoint, the pyrrole moiety seems to wedge between the Phe1236 and Lys1237 residues. Binding of BTX is stabilized by interactions with the phenylalanine residue (Phe1236). BTX also attracts the lysine residue (Lys1237) and alters its original configurations predicted for the tetrodotoxin receptor (Tikhonov and Zhorov, 2005a).

Monte Carlo minimization docking of BTX in the F1236K mutant starting from the ligand position energetically optimal in the wild-type channel predicts that F1236K destabilizes the ligand-channel complex for two main reasons. First, hydrophilic amino group of F1236K binds to the hydrophobic side of BTX, which is energetically unfavorable (Fig. 7B). Second, the electrostatic repulsion between the amino group of F1236K and the protonated amino group of BTX is observed (Fig. 7B). A substitution of residue Phe1236 with R destabilizes BTX binding by similar mechanisms.

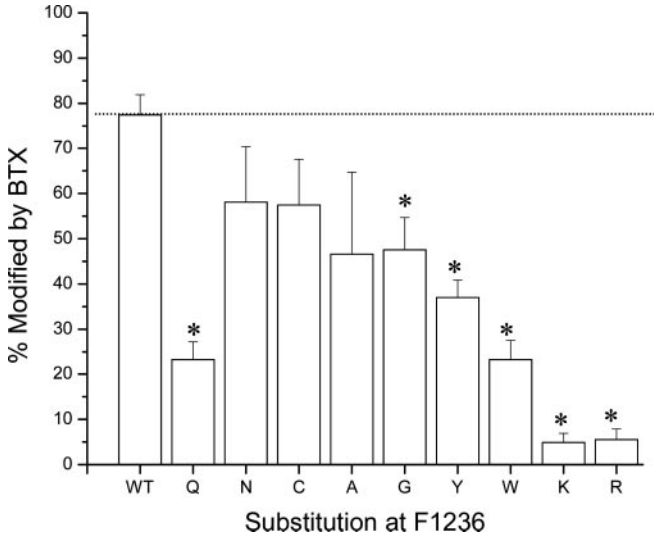

Fig. 5. Relative magnitude of modification by BTX among various rNav1.4-Phe1236 mutants. The amplitudes of maintained Na^+ currents at the end of the +50-mV pulse were measured after 1000 repetitive pulses, normalized with respect to its peak amplitude, and plotted against the mutated residue (n = 3–7). Notice that rNav1.4-F1236R and F1236K are severely resistant to BTX modification (n = 5). *, $P < 0.05$ compared with the value of the wild-type.

Discussion

This report provides first experimental evidence that mutations of Phe1236 at the P-loop of the Na^+ channel could strongly affect BTX binding. The phenylalanine residue adjacent to the DEKA selectivity filter is conserved in all Na^+ channel isoforms (Nav1.1–1.9). We have thus successfully applied a reverse engineering approach to a structural model generated by computer simulation. This structural model is consistent with the hypothesis that BTX is bound within the inner cavity as suggested earlier by site-directed mutagenesis (Wang and Wang, 2003).

The BTX Orientation along Its Binding Site within the Inner Cavity. Among various ligands that modify voltage-gated Na^+ channels, BTX is one of the most versatile. It affects almost every aspect of the Na^+ channel functions. Because BTX alters Na^+ channel functions in so many ways, it was reasonable to speculate that some, if not all, BTX actions are allosteric in nature (Catterall, 1980; Strichartz et al., 1987). In addition, because BTX is highly hydrophobic and could penetrate the lipid bilayer, it has been postulated that BTX binds to the Na^+ channel at the protein/lipid interface (Brown, 1988), far away from the central pore. On the other hand, BTX could embed within the hydrophobic pocket of the Na^+ channel protein (Hille, 2001).

In theory, receptor mapping of BTX by the site-directed mutagenesis should help understand how BTX works within the Na^+ channel. Unfortunately, such efforts have created more puzzles. For example, BTX was found neither at the

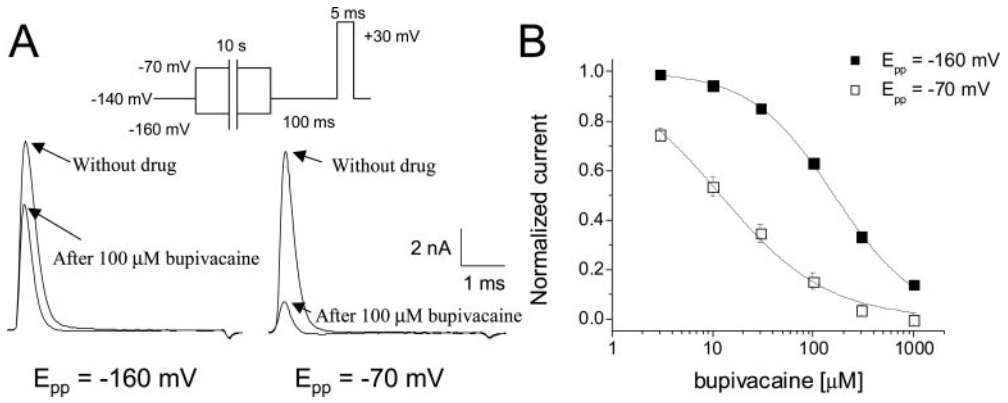

Fig. 6. Resting- and inactivated-channel block of rNav1.4-F1236K mutant by bupivacaine. A, top, the pulse protocol consisted of a 10-s conditioning pulse (E_{pp}) to −160 mV (resting-channel block) or −70 mV (inactivated-channel block) followed by a 100-ms interval at −140 mV, and a subsequent test pulse to +30 mV. A, bottom, superimposed current traces were shown before and after 100 μM bupivacaine with Epp at −160 mV (left) and at −70 mV (right), respectively. B, bupivacaine dose-response curves for resting and inactivated channels. The peak current at various concentrations of bupivacaine was normalized to the control response without drug, plotted against concentration, and fitted with a Hill equation. The IC_{50} value for the resting channels was 162.3 ± 3.3 μM (Hill coefficient, 1.04 ± 0.06) (■, n = 5) and for inactivated channels was 12.1 ± 0.9 μM (Hill coefficient, 0.85 ± 0.05) (□, n = 5).

protein/lipid interface nor within a hydrophobic pocket. Instead, BTX was mapped within the water-filled inner cavity of the Na^+ channel, clearly inconsistent with the earlier predictions. The BTX orientation and its contact points with the channel become crucial in explaining how BTX renders the channel open persistently and how ions permeate within BTX-modified Na^+ channels. Our data support the contention that the Phe1236 residue interacts with the distal pyrrole moiety of BTX (Fig. 1A), as predicted by computer modeling (Fig. 7A). This interaction requires that the side chain of the phenylalanine residue (Phe1236) face the inner pore. The stacking role of the pyrrole moiety is therefore consistent with the equal potency of batrachotoxinin A 20-α-benzoate (Brown, 1988), because the substituted benzene group can stack with Phe1236. Also consistent with this pyrrole-binding model is the fact that no biological activity has been found for batrachotoxinin A, which lacks the pyrrole moiety. It is noteworthy that a previous report showed that F1236C mutant channels are sensitive to a cysteine-modifying reagent, MTSEA, applied to the outside of the cell but not to MTSEA applied to the inside (Yamagishi et al., 1997). These authors suggested that F1236C is facing the external surface of the Na^+ channel and that the K^+ channel model of the P-loop that span the selectivity region may not be applicable to the Na^+ channel. To resolve this discrepancy, Tikhonov and Zhorov (2005a) proposed that an MTSEA drug pathway to the inner pore exists between the interface of the D3 and the D4 in the Na^+ channel.

As shown in Fig. 5, the BTX sensitivity followed the order Phe1236 > Asn ≈ Cys > Gly ≈ Ala > Tyr > Gln ≈ Trp > Arg ≈ Lys. Aromatic substitutions Tyr and Trp showed unexpected and considerable resistance to BTX modification ($P < 0.05$) whereas wild type with Phe is highly sensitive to BTX. A possible explanation of this paradox was found in the analysis of the model of the F1236K mutant with BTX. The structural model predicts that ligand-receptor energy is destabilized because of screening of the hydrophilic F1236K by the hydrophobic face of BTX (Fig. 7B). Binding of the hydrophobic face of BTX to Tyr and Trp could also screen the polar groups of these residues from water (hydrophobicity scale: Phe > Trp > Tyr), the energetically unfavorable situation. Short N could escape the screening more easily than bulky Tyr/Trp and long Gln, Arg, and Lys. Another possibility is that the polar groups in large residues could form H-bonds with the carbonyl oxygen at the pyrrole moiety before it reaches the DEKA locus. As a result, BTX would not get deep inside the pore to realize its binding potential. At present, it is difficult to distinguish among these various possibilities because details of the interactions among flexible residues of the channel and flexible fragments of the ligands cannot be predicted unambiguously without knowing the X-ray structure of the Na^+ channel.

How BTX Reduces the Single Channel Conductance. It seems contradictory that BTX binds in the pore and simultaneously maintains the conductance. Why does BTX not block the channel fully like lidocaine, a local anesthetic that also binds within the inner cavity? In fact, it is baffling that BTX, with a molecular weight of 538.68, almost twice as large as lidocaine (234.34) or bupivacaine (288.43), does not block the channel.

It is well documented that Na^+ channel activators are amphiphilic and have their polar groups clustered at one side of the molecules (Masutani et al., 1981; Codding, 1983; Kosower, 1983). For example, one face of BTX is hydrophobic, whereas the opposite face is hydrophilic. In contrast, various channel blockers, including local anesthetics, lack such a polar side. It is likely, therefore, that the hydrophobic face of BTX may bind to the hydrophobic side of the pore wall (Fig. 7A), in particular to segment D4S6 containing Phe1579. This phenylalanine residue is indeed critical for binding of both BTX and local anesthetics.

In such an orientation, the hydrophilic face of the agonist would occur against the hydrophilic Asn784 in D2–S6, as shown in the computer model (Fig. 7A). Such a BTX binding mode would allow Na^+ ions to flow between the hydrophilic face of the ligand and hydrophilic residues at the channel wall (Tikhonov and Zhorov, 2005b). The width of this hydrophilic lumen is not smaller than that in the selectivity filter in K^+ channels. Indeed, the ion permeation through the hydrophilic lumen between the BTX and the inner pore wall differs from permeation through the nonmodified channel. Ion permeation is normally facilitated by the pore-helix ma-

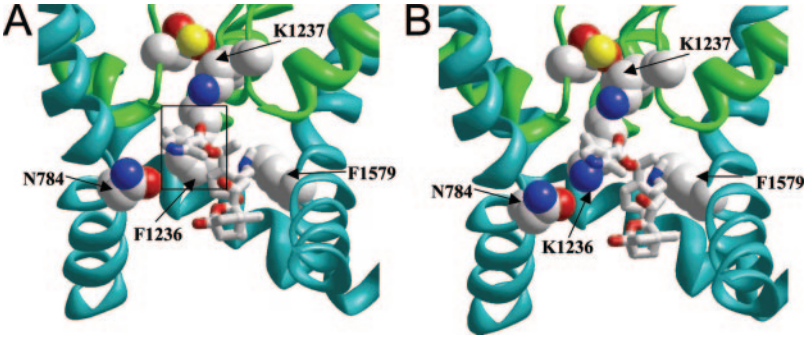

Fig. 7. Monte Carlo-minimized models of the open Na^+ channel with BTX. Pore helices and P-loop turns are shown as green ribbons and rods, respectively. The inner helices are shown as cyan ribbons. Domain 1 and the outer helices are not shown for clarity. Side chains of Asn784 (D2S6), Phe1579 (D4S6), and Phe1236 (D3/P-loop) and residues in the DEKA locus are space-filled. The Na^+ ion in the selectivity filter is colored yellow. Carbon, nitrogen, and oxygen atoms are colored gray, blue, and red, respectively. For clarity, hydrogen atoms are not shown. The models were built and Monte Carlo-minimized as described elsewhere (Tikhonov and Zhorov, 2005a,b). A, BTX bound within rNav-1.4. The ligand is shown as sticks. The hydrophobic face of the ligand interacts with Phe1579. Residue Phe1236 is in box. An interface between the polar face of BTX and Asn784 may serve as a hydrophilic pathway for the permeating ions in BTX-modified channels. The hydrogen bond between BTX and Lys1237 displaces the latter from orientation optimal in BTX-free channel. B, BTX in the inner cavity of the rNav-1.4/F1236K mutant without phenylalanine/pyrrole stacking. The unfavorable dehydration of K1236 as well as electrostatic repulsion between F1236K and the protonated amino group of BTX exert destabilizing influences on the ligand-receptor binding.

crodipoles focused at the pathway axis (Doyle et al., 1998). In the presence of BTX, the ion pathway is redirected: Na^+ ions do not flow through the focus of the helix macrodipoles, and the benefits of helix dipoles are not realized. As a result, conductance of the agonist-activated sodium channels is reduced.

How BTX Alters Ion Selectivity. Preliminary results showed that mutants K1237W and K1237R are functional and remain sensitive to BTX modification. Because Trp is relatively bulky, this substitution is again consistent with an unoccupied space between Phe1236 and Lys1237 residues (Fig. 7A). If the position and the orientation of BTX with the pore region are as predicted in Fig. 7A, it is then possible to speculate how BTX could alter ion selectivity via interacting with Phe1236 and Lys1237 residues. The pyrrole moiety of BTX is electron-rich and therefore partially negative. With this aromatic π electron cloud, pyrrole becomes a good candidate for stacking with Phe1236 (Fig. 7A), so that the pyrrole moiety will be affixed. A hydrogen bond may then be formed between the amino group of the lysine side chain and the carbonyl group attached to the pyrrole group of BTX. Interactions between Lys1237 and BTX (Fig. 7A) would distort the Lys1237 orientation and widen the DEKA locus. Such a widening of the selectivity filter by BTX has been suggested previously (from $\sim 3 \times 5$ Å to $\sim 3.8 \times 6$ Å; Khodorov, 1978) and would permit the larger cations NH_4^+ and Tl^+ to pass through with a high permeability ratio. We do not know precisely how these ions permeate via the BTX-bound inner cavity. Additional simulations using these ions are desirable. However, in the absence of the X-ray structure of the Na^+ channel, results of such simulations would remain questionable.

How BTX Affects Channel Gating. Earlier simulations have shown that even though BTX could be trapped in the closed conformation of the Na^+ channel, the channel is destabilized by BTX, which is too large to fit nicely in the water-filled cavity of the closed channel (Tikhonov and Zhorov, 2005b). The computer model suggests two possible mechanisms to explain the shifts in the voltage dependence for activation by BTX. First, BTX could prevent the activation gate from closing. This becomes feasible if elongated BTX is aligned along the open pore with strong binding to residues at the C-terminal ends of S6 segments. A part of the BTX molecule may reach position 21 at D1S6 (Fig. 1C; L437) (Wang and Wang, 2003), which could be very close to the activation gate of the Na^+ channel. Second, a strong binding between BTX and up to four S6 segments may provide sufficient free energy to stabilize the open conformation of the Na^+ channel. In particular, BTX could stabilize the bent configuration of S6 segments, because residues adjacent to the gating hinges (Gly/Ser residues), Ser1276 and Phe1579, form a part of the BTX receptor. It is likely that a combination of these mechanisms work together to stabilize the open state. Thus, BTX shifts the equilibrium between the closed and open states of the channel in favor of the open states. As a result, BTX-bound channels open in response to a weaker stimulus and stay open longer than nonmodified channels. However, it remains unclear how BTX eliminates both fast and slow inactivation gating processes during prolonged depolarization. The receptor for the fast-inactivating particle has not been delimited (Catterall, 2000), although BTX might directly interfere with the binding of the fast-inactivating particle to its receptor. In addition, mechanisms for the slow inactivation gating are largely unknown, but rearrangement at the P-loop domain has been implicated to play a critical role (Ulbricht, 2005). Our finding that BTX directly interacts with the P-loops in the immediate proximity to the selectivity filter suggests that ligand binding to the P-loop may prevent conformational transitions associated with the slow inactivation.

Summary. Our present study with site-directed mutagenesis of rNav1.4-Phe1236 residue supports the stacking model of the BTX pyrrole moiety presented in Fig. 7A. Such a model is consistent with the hypothesis that BTX binds within the inner cavity. This receptor-ligand model readily explains the key features of BTX-modified sodium channels, including how BTX directly affects Na^+ channel permeation/selectivity and how BTX directly shifts the activation gating. The hypothesis that BTX acts allosterically has become less likely for these diverse BTX actions. Nevertheless, without knowing the X-ray structure of the Na^+ channel, reliance upon computer-generated structural models must be undertaken with caution. Further elucidation of this structural model is justified to explain how BTX eliminates both fast and slow inactivation gating. Such experiments will help explain how bound BTX continuously maintains the Na^+ channel conductance during prolonged depolarization.

Acknowledgments

We thank Dr. John Daly for providing batrachotoxin.

References

Brown GB (1988) Batrachotoxin: a window on the allosteric nature of the voltage-sensitive sodium channel. *Int Rev Neurobiol* **29:**77–116.
Catterall WA (1980) Neurotoxins that act on voltage-sensitive sodium channels in excitable membranes. *Annu Rev Pharmacol Toxicol* **20:**15–43.
Catterall WA (2000) From ionic currents to molecular mechanisms: the structure and function of voltage-gated sodium channels. *Neuron* **26:**13–25.
Codding PW (1983) Structural studies of channel neurotoxins. 2. Crystal structure and absolute configuration of veratridine perchlorate. *J Am Chem Soc* **105:**3172–3176.
Correa AM, Latorre R, and Bezanilla F (1991) Ion permeation in normal and batrachotoxin-modified Na^+ channels in the squid giant axon. *J Gen Physiol* **97:**605–625.
Daly JW, Myers CW, and Warnick JE (1980) Levels of batrachotoxin and lack of sensitivity to its action in poison-dart frogs (*Phyllobates*). *Science (Wash DC)* **208:**1383–1385.
Doyle DA, Cabral JM, Pfuetzner RA, Kuo A, Gulbis J, Cohen S, Chait BT, and MacKinnon R (1998) The structure of the potassium channel: molecular basis of potassium conduction and selectivity. *Science (Wash DC)* **280:**69–77.
Hamill OP, Marty E, Neher ME, Sakmann B, and Sigworth FJ (1981) Improved patch-clamp techniques for high-resolution current recording from cells and cell-free membrane patches. *Pflueg Arch Eur J Physiol* **391:**85–100.
Hille B (2001) Modification of gating in voltage-sensitive channels, in *Ion Channels of Excitable Membranes,* pp 635–662, Sinauer Associates Inc., Sunderland, MA.
Jiang Y, Lee A, Chen J, Cadene M, Chait BT, and MacKinnon R (2002) The open pore conformation of potassium channels. *Nature (Lond)* **417:**523–526.
Khodorov BI (1978) Chemicals as tools to study nerve fiber sodium channels: effect of batrachotoxin and some local anesthetics. *Prog Biophys Mol Biol* **45:**153–174.
Kosower EM (1983) A hypothesis for the mechanism of sodium channel opening by batrachotoxin and related toxins. *FEBS Lett* **163:**161–164.
Krueger BK, Worley JF, and French RJ (1983) Single sodium channels from rat brain incorporated into planar lipid bilayer membranes. *Nature (Lond)* **303:**172–175.
Li H-L, Hadid D, and Ragsdale DS (2002) The batrachotoxin receptor on the voltage-gated sodium channel is guarded by the channel activation gate. *Mol Pharmacol* **61:**905–912.
Linford NJ, Cantrell AR, Qu Y, Scheuer T, and Catterall WA (1998) Interaction of batrachotoxin with the local anesthetic receptor site in transmembrane segment IVS6 of the Voltage-gated sodium channel. *Proc Natl Acad Sci USA* **95:**13947–13952.
Masutani T, Seyama I, Narahashi T, and Iwasa J (1981) Structure-activity relationship for Grayanotoxin derivatives in frog skeletal muscle. *J Pharmacol Exp Ther* **217:**812–819.
Nau C and Wang GK (2004) Interactions of local anesthetics with voltage-gated Na^+ channels. *J Membr Biol* **201:**1–8.
Nau C, Wang S-Y, Strichartz GR, and Wang GK (1999) Point mutations at N434 in

D1–S6 of μ1 Na^+ channels modulate potency and stereoselectivity of local anesthetic enantiomers. *Mol Pharmacol* **56:**404–413.
Strichartz GR, Rando TA, and Wang GK (1987) An integrated view of the molecular toxinology of sodium channel gating in excitable cells. *Annu Rev Neurosci* **10:**237–267.
Sunami A, Dudley SC Jr, and Fozzard HA (1997) Sodium channel selectivity filter regulates antiarrhythmic drug binding. *Proc Natl Acad Sci USA* **94:**14126–14131.
Tikhonov DB and Zhorov BS (2005a) Modeling P-Loops domain of sodium channel: Homology with potassium channels and interaction with ligands. *Biophys J* **88:**184–197.
Tikhonov DB and Zhorov BS (2005b) Sodium channel activators: model of binding inside the pore and a possible mechanism of action. *FEBS Lett* **579:**4207–4212.
Tokuyama T, Daly J, Witkop B, Karle IL, and Karle J (1968) The structure of batrachotoxinin a, a novel steroidal alkaloid from the Colombian arrow poison frog, *Phyllobates aurotaenia*. *J Am Chem Soc* **90:**1917–1918.
Ulbricht W (2005) Sodium channel inactivation: molecular determinants and modulation. *Physiol Rev* **85:**1271–1301.
Wang S-Y, Bonner K, Russell C, and Wang GK (2003) Tryptophan scanning of D1S6 and D4S6 C-termini in voltage-gated sodium channels. *Biophys J* **85:**911–920.
Wang S-Y and Wang GK (2003) Voltage-gated sodium channels as primary targets of diverse lipid-soluble neurotoxins. *Cell Signal* **15:**151–159.
Yamagishi T, Janecki M, Marban E, and Tomaselli GF (1997) Topology of the P segments in the sodium channel pore revealed by cysteine mutagenesis. *Biophys J* **73:**195–204.

Address correspondence to: Ging Kuo Wang, Department of Anesthesia, Brigham and Women's Hospital and Harvard Medical School, Boston, MA 02115. E-mail: wang@zeus.bwh.harvard.edu